MID-CRUSTAL FOCUSED FLUID MOVEMENT: THERMAL CONSEQUENCES AND SILICA TRANSPORT

14

James A. D. Connolly

14.1 INTRODUCTION

Petrologic evidence indicates that a fluid phase is almost invariably present during metamorphic activity. This association has led some petrologists to conclude that fluids are, at least sometimes, a source of metamorphic heat. An alternative view is that the association of fluids and metamorphic activity reflects the catalytic, rather than causal, role of fluids in metamorphism. This latter view is supported by numerical modelling of crustal metamorphism which suggests that regional-scale metamorphic fluid fluxes, estimated to be on the order of 10^{-8} to 10^{-10} kg m^{-2} s^{-1}, are too small to significantly alter the thermal development of metamorphic systems (e.g. Peacock, 1987, 1989; Brady, 1989; Connolly and Thompson, 1989; Jamtveit, Bucher-Nurminen and Austrheim, 1990). Thus, it appears that anomalously large fluxes are required to generate notable thermal effects. Such large fluxes may be attained if mantle sources comprise a major component of metamorphic fluid budgets (Ganguly, Singh and Ramana, 1995), but the fluid compositions in this case are likely to be atypical of crustal metamorphism. This study examines the hypothesis that large-scale fracture systems are capable of generating fluid fluxes adequate to cause localized heating at crustal depths (> 10–12 km) where free-convection is unlikely. Such fracture systems have been hypothesized to explain 'metamorphic hot spots' in New England (Chamberlain and Rumble, 1988), where metamorphic rocks apparently show evidence of heating independently of any regional or magmatic source.

The thermal consequences of channelized fluid flow in two-dimensional parallel fractures have been examined in detail by Brady (1989) and Hoisch (1991) who present numerical and analytical solutions for the thermal profile about fluid channels. Brady's work has a number of interesting implications, perhaps the most important of which is that even accepting high estimates for regional fluid fluxes, metamorphic fluids must be focused into widely spaced channels (separated by > 2 km) to raise the temperature of the rocks in the vicinity of the channel more than 10 K above the inter-channel rock temperature. Brady's analytical solutions also show that given a constant total flux (i.e. integrated over channel width), variation in channel width has little effect on the temperature distribution around the channel provided this width is small ($\leqslant 10\%$) in comparison to the channel spacing. This is useful because it means that it is not necessary to understand the details of fluid flow, i.e. whether the flow is focused into a single conduit or it is spread out over a broad fracture zone, assuming local thermal equilibrium is maintained.

For fracture fluid flow to be an effective heat transfer mechanism, hot fluids must be focused into a fracture zone at depth, channelled upwards,

and dispersed in cool shallower rocks. The process of dispersion is important for two reasons; it acts as a 'thermal brake' that allows the fluid to cool rapidly; and it could explain pervasive veining and re-equilibration which would otherwise not be expected. This study extends Brady's and Hoisch's analyses to account for these processes, and in many ways parallels the treatment by Pedersen, Johansen and Wangen (Chapter 13) of fracture confined flow in sedimentary basins. In addition, radially symmetric focusing and mid-crustal granitic plutonism are considered here. These processes are potentially more effective mechanisms for generating high fluid fluxes than the channelling of fluid from regional devolatilization into planar fractures as discussed by Brady (1989). Silica transport through deep crustal fracture zones has also been proposed as a means of explaining pervasive quartz vein formation (e.g. Walther and Orville, 1982; Yardley, 1986), and the models employed here can be used to test this hypothesis.

It has been recognized for some time that high fluid fluxes can be generated by free-convection around shallow cooling plutons (Norton and Knight, 1977). Whether free-convection occurs at greater depths is more controversial, it will depend on the degree to which connected porosity or fracture networks can be maintained, and therefore on rheology. Rocks at depths of greater than 10 km are likely to be too plastic during prograde metamorphism to allow large-scale free-convection. In the absence of fracture networks, permeability variation resulting from lithological heterogeneity will further impede free-convection (Bjørlykke, Mo and Palm, 1988). Thus it is unlikely that free-convection at depth can be very effective heat transfer mechanism, moreover the heating effect of free-convection would be diffuse and difficult to recognize. For these reasons, free-convection is not considered here. It is noteworthy though, that small-scale free-convection cells as suggested by Etheridge, Wall and Vernon (1983, cf. Connolly and Ko, 1995) could be a mechanism for producing pervasive quartz veining, which is difficult to explain on the basis of one-pass fluid flow models (Yardley, 1986; Connolly and Thompson, 1989).

The present study, as those of Brady (1989) and Hoisch (1991), evaluates the effects of focused fluid flow, without considering the more fundamental question of how focusing may arise. Matthai and Roberts (Chapter 16) and Thompson (Chapter 17) address aspects of this question in this volume.

14.2 FOCUSED REGIONAL METAMORPHIC FLUID

There is considerable evidence for fracture channelization of fluids released by metamorphic devolatilization on a scale of 0.1–1 km (e.g. Oliver *et al.*, 1993); and Skelton, Graham and Bickle (1995) have demonstrated a four-fold increase in integrated fluid fluxes that occurred in response to lateral focusing of metamorphic fluid over distances approaching 10 km by an antiformal structure. Unfortunately, there is little, if any, direct evidence of the scale or geometry of fluid channels associated with thermal anomalies, except at shallow levels in the crust (e.g. Mickucki and Heinrich, 1993). However, if the 'metamorphic hot spots' of Chamberlain and Rumble (1988) are indeed the result of fluid channelling then they provide a number of constraints on the process of their formation. In the case they describe in detail, the Bristol hotspot, Chamberlain and Rumble estimate that the hotspot formed at a depth of *c.* 12 km and raised the rock temperatures to about 973 K, *c.* 300 K above the background temperature of 673 K. This implies a normal geothermal gradient of 33 K km^{-1}, and, if the fluids were generated by dehydration, a minimum depth of the fluid source of *c.* 22 km. The Bristol hotspot is roughly 6 × 10 km in map section and evidence of hydrothermal activity (veins and isotopic re-equilibration) is present throughout, suggesting that the fluids were dispersed throughout the hotspot.

14.2.1 REGIONAL METAMORPHIC FLUID FLUX

If the source of the fluids responsible for the Bristol hotspot was water released by dehydration, the dehydration must have occurred at temperatures

in excess of 973 K and at pressures of greater than 8 kbar[1]. Ignoring the difficulty of producing free water at these conditions in sialic material, a possible water source would be biotite dehydration. An estimate of the upper limit of fluid production by such a reaction can be obtained by assuming a (high) biotite mode of about 25 wt%, combined with a rapid rate of isograd advance, for a high temperature reaction, of 4×10^{-11} m s^{-1} (1.3 km Ma^{-1}, e.g. Thompson, 1989; Connolly and Thompson, 1989), this yields a flux of 10^{-9} kg m^{-2}s^{-1}, designated here q^*. Real fluxes are likely to be highly variable, but generally smaller, as most hydroxylated silicates, notably amphibole, contain less water. For comparison, most authors have estimated regional fluid fluxes less conservatively to be on the order of $10\,q^*$ (Walther and Orville, 1982; Peacock, 1989; Brady, 1989), whereas Connolly and Thompson (1989) suggested average metamorphic fluxes of $< 0.2\,q^*$. From field evidence, Skelton, Graham and Bickle (1995) estimated the unfocused regional integrated fluxes to be on the order of 10^5 kg m^{-2}, this integrated flux would be realized at q^* in *c.* 3 Ma, a relatively short time in the context of regional metamorphism.

Similar fluxes are derived given the assumption that the time-scale of whole-crustal metamorphism is ultimately determined by heat conduction (England and Thompson, 1984). In this case the metamorphic time-scale is:

$$\tau_M \approx \frac{l_c^2}{2}\kappa \qquad (14.1)$$

where l_c and κ are the crustal thickness and thermal diffusivity (Table 14.1). If the weight fraction of volatiles lost from the metamorphic pile is X_v, then the time-averaged fluid flux is:

$$\hat{q} = \frac{l_c X_v}{\tau_M} = \frac{X_v 2\kappa}{l_c} \qquad (14.2)$$

Pelitic crust loses about 3 wt% volatiles in the transition from lower greenschist to granulite facies (Fyfe, Price and Thompson, 1978). Thus for crustal thicknesses characteristic of extensional (10 km), thermal (35 km), and collision belt metamorphism (70 km), $\hat{q} = 2\text{–}8 \times 10^{-9}$ kg m^{-2}s^{-1}. This time-averaged flux would be obtained at the top of the metamorphic pile, consequently average fluxes deeper within the pile could be substantially lower (cf. Connolly and Thompson, 1989). It is interesting to observe that if fluid pressure during metamorphism is near lithostatic, as inferred from phase equilibria (e.g. Fyfe, Price and Thompson, 1978) rearrangement of Darcy's law:

$$k_h = \hat{q}\left(\frac{\mu_f}{\rho_f g \Delta\rho}\right) \qquad (14.3)$$

requires metamorphic permeabilities to be on the order of 10^{-20} m^2. In equation 14.3 μ_f is the fluid viscosity (10^{-4} Pa s, Walther and Orville, 1982), $\Delta\rho$ is the difference between the fluid and rock density (2×10^3 kg m^{-3}), and $g\Delta\rho$ is the pieziometric gradient.

For the distance scales $h \approx 10$ km considered here a minimum estimate of the focusing necessary for significant heat convection can be estimated by determining conditions such that thermal Peclet number:

$$\mathrm{Pe} = \frac{hq}{\rho_f \kappa} \qquad (14.4)$$

for one-dimensional flow is of the order of 1 (Bickle and McKenzie, 1987). This approach yields focusing factors of the order of 100 for a regional flux of q^*, but is likely to significantly underestimate the actual focusing required in the limit that the fracture zone is narrow (< 50 m) because the fracture system then loses a substantial amount of heat by conduction to the wall rocks.

[1] Chamberlain and Rumble (1988) estimated metamorphic temperatures from the garnet–biotite geothermometer, differences in the calibrations of this geothermometer suggest the possibility of considerable systematic error in its use. Thus it may be more important to consider the reported temperatures differences, rather than the absolute temperatures. Systematically lower temperatures, would require less extreme conditions for fluid generation, but would not otherwise substantially effect the model results presented here.

14.2.2 FLUID FOCUSING AND DISPERSION

The models illustrated in Fig. 14.1 have been adopted to simulate the collection and dispersion of fluid produced along a metamorphic dehydration reaction front into a planar or radially symmetric fracture zone. For brevity these models are referred to as 'crack' and 'pipe' flow models. In both models, fluids at depth are collected from a horizontal region of width $\pm W$ at depth Y_f, Fig. 14.1 (i.e. a dehydration reaction front). Once collected within this region the fluid is gradually focused into the fracture within the inverted trough or cone-shaped region truncated by the base of vertical fracture zone ($\pm w$ at Y_b). At any point within this region, except along the axis of the fracture zone, the flux will have a lateral component, fluxes outside this region are assumed to have no lateral component.

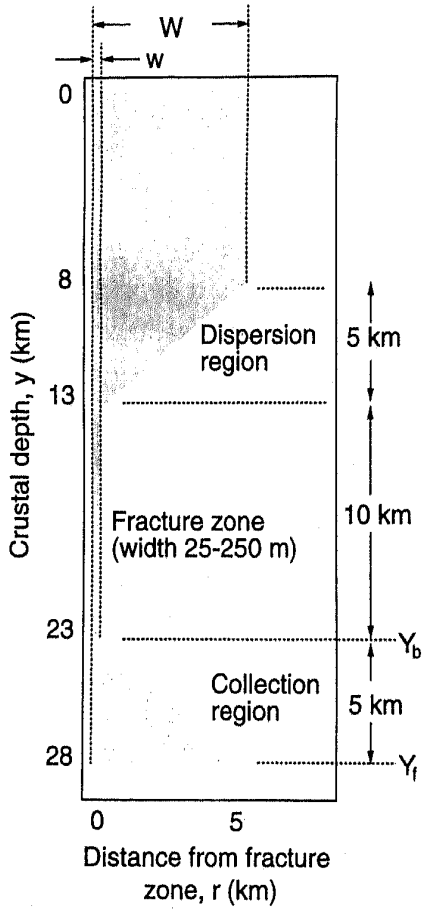

Figure 14.1 Geometry of models for focusing and dispersion of metamorphic fluid. The pipe model has radial symmetry about the fracture zone axis, and the crack model has mirror symmetry perpendicular to the fracture plane.

The efficiency of fluid catchment would be expected to vary with lateral distance from the fracture zone axis, being unity directly below the fracture zone, and decreasing asymptotically away from the zone. Because low fluxes are unimportant in heat and mass transport, this distribution can be represented by the catchment efficiency, E, where:

$$E = \cos\left(\frac{\pi r}{2W}\right) \tag{14.5}$$

where r is the lateral distance from the fracture zone axis. Equation 14.1 yields an efficiency of 1 at $r = 0$ and zero at $r = \pm W$. Integrating equation 14.1 over the entire width of the catchment zone yields total catchment efficiencies, $\hat{E}$, of 63.7% $\left(\frac{2}{\pi}\right)$ and 46.3% $\left(\frac{4}{\pi}\left[1 - \frac{2}{\pi}\right]\right)$, for the crack and pipe model symmetries, respectively. The vertical (q_y) and horizontal (q_r) steady-state flux components consistent with these assumptions within the focusing region are then:

$$q_y = A\cos\left(\frac{\pi r}{2u}\right) \tag{14.6}$$

and

$$q_r = A\frac{r}{\delta y}\cos\left(\frac{\pi r}{2u}\right) \tag{14.7}$$

where $\delta y = y - Y_b$ and u is the width of the focusing region at depth y, i.e. $u = W\,\delta y/(Y_f - Y_b)$. The parameter A in equations 14.6 and 14.7 is model-dependent, for a planar fracture zone:

$$A = \frac{Q\pi}{4u} \tag{14.8}$$

where Q, the total vertical flow rate through the fracture zone, is:

$$Q = 2W\hat{E}q \tag{14.9}$$

For a radially symmetric fracture zone:

$$A = \frac{Q}{\left(1 - \frac{2}{\pi}\right)4u^2} \tag{14.10}$$

and

$$Q = \pi W^2 \hat{E} q \qquad (14.11)$$

The dispersion process is assumed to be the inverse of collection, applying equations 14.6 and 14.7 with the appropriate modification. The component of the regional flux that is not focused is ignored. This component is small in comparison to the fluxes obtained for any significant focusing, and so may be discounted without important consequences.

Although equation 14.5 is arbitrary, it is probably not a large component of the uncertainty in the models. The parameters chosen to describe the shape of the focusing and dispersion regions are more important. In the limit that all fluid produced along a reaction front flows laterally into a fracture zone, the focusing process will be isothermal and results in the highest possible fluid temperatures within the vertical fracture zone. Indirect evidence for bedding plane channelling of fluids within dehydrating rock has been observed (e.g. Ferry, 1987; Skelton, Graham and Bickle, 1995) for rocks metamorphosed at crustal depths > 12 km. It is difficult to extract flux components from these studies, but strong lateral channelling in the lower crust would require large permeability contrasts and lateral fluid pressure gradients. Lateral fluid pressure gradients can be maintained only if rock viscosity is low, but at the high temperature–pressure conditions necessary to produce fluids capable of generating a metamorphic hotspots rocks are likely to deform rapidly. In view of this, it is assumed here that the lateral flux component is generally smaller than the vertical component.

The width of fluid focusing regions is difficult to constrain, a maximum width is given by the spacing of Chamberlain and Rumble's (1988) hotspots. This width, *c.* 25 km, is inconsistent with the assumption that the lateral flux components are smaller than the vertical flux components. In contrast to the focusing problem, the width of the dispersion region is defined by Chamberlain and Rumble's hotspots by the extent of hydrothermal veining. This veining extends over an area of about 10 km^2 and indicates a minimum dispersion region width of 3 km. In most of the model results presented here, a 5 km width (W) for the dispersion region is assumed, and for the sake of simplicity the same width is used for the focusing region. The effect of larger widths for the focusing region will be simulated by increasing the value of the regional flux. For example, focusing with $W = 5$ km and $q = 10\,q^*$ is roughly equivalent to $W = 50$ km and $q = q^*$ for a planar fracture model (equation 14.9), or $W = 15$ km and $q = q^*$ for radially symmetric flow (equation 14.11).

Brady's (1989) equations show that the effect of the width of the fracture zone is relatively minor (see also below), thus unless otherwise noted a constant width of 500 m is used here (i.e. $w = 250$ m).

14.2.3 SOLUTION OF THE ENERGY CONSERVATION EQUATION

The heat transfer coefficient for fluid–rock heat transfer (Ozisik, 1985) is unlikely to differ significantly from unity for plausible fracture widths (e.g. Norton and Knapp, 1970). It follows that true adiabatic fluid flow can be excluded from consideration; therefore, only equilibrium heat flow models are applied here. The thermal consequences of focused steady-state fluid flow were calculated by solving the energy conservation equation:

$$C_{rx}\frac{dT}{dt} = k\left[\nabla^2 T + \frac{p}{r}\left(\frac{\partial T}{\partial r}\right)\right] - C_f q \nabla T \qquad (14.12)$$

where p is zero and one for the planar and radial symmetries, respectively (see Table 14.1 for symbols and parameter values). Stable numeric solutions of equation 14.12 are difficult to obtain by standard finite difference techniques because of strong spatial variations in the model fluid fluxes and high Courant numbers. The techniques employed to circumvent these problems are described in the Appendix.

Constant temperature boundary conditions were assigned for horizontal boundaries the vertical boundaries of radially symmetric models.

Table 14.1 Frequently used symbols and characteristic values

Symbol	*Meaning*	*Units*	*Characteristic value*
C_{rx}	rock specific heat	$J m^{-3} K^{-1}$	2.5×10^6
C_f	fluid heat capacity	$J kg^{-1} K^{-1}$	4×10^3
$\hat{E}$	integrated catchment efficiency, planar symmetry	0.636	
$\hat{E}$	integrated catchment efficiency, radial symmetry	0.463	
k	thermal conductivity	$W m^{-1} K^{-1}$	2.25
L	latent heat of melting	$J kg^{-1}$	2×10^5
q	unfocused fluid mass flux rate	$kg m^{-2} s^{-1}$	
q^*	expected maximum q	$kg m^{-2} s^{-1}$	10^{-9}
p	symmetry flag, planar symmetry		0
p	symmetry flag, radial symmetry		1
Q	fluid mass flow rate	$kg m^{p-1} s^{-1}$	
r	horizontal distance coordinate	km	
t	time	s, a, ka, Ma	
T	temperature	K	
W	half-width of focusing/dispersion region	km	5
w	half-width of fracture zone	km	0.025–1
y	depth	km	
κ	thermal diffusivity	$m^2 s^{-1}$	1.1×10^{-6}
ρ_f	fluid density	$kg m^{-3}$	$0.7–0.9 \times 10^3$
ρ_{rx}	rock density	$kg m^{-3}$	2.8×10^3

No-flow (mirror symmetry) conditions were used for the planar fracture models. In solving equation 14.12, the movement of the reaction front and other effects of dehydration (enthalpy, compaction, mass loss, etc.) were ignored. This is justified given the relatively short time-scale for the formation of advected heat anomalies (*c.* 10^4 a) in comparison to that for reaction effects (Connolly and Thompson, 1989). Furthermore, because regional metamorphic dehydration rates are likely to be controlled by heat flow and therefore near equilibrium (e.g. Yardley, 1986), the dehydration process will be essentially isothermal, as modelled here, regardless of endothermic dehydration effects. Variation in the conductivity, density and specific heats of the fluid and rock due to temperature or fluid/rock proportions were not considered, these effects are small and would be difficult to evaluate precisely. Accuracy of the numerical solutions was tested by evaluting the energy conservation constraints, and by changing the node spacings employed. For all accepted solutions the instantaneous and cumulative energy conservation constraints were satisfied to within a tolerance of 0.1% of the energy transfer.

14.2.4 SILICA PRECIPITATION AND THROTTLING EFFECTS

To estimate the amount of silica transported and precipitated by focusing of metamorphic fluid, the fluid was assumed to be essentially pure water and saturated with respect to quartz. The equilibrium rate of quartz precipitation, $\dot{s}$, was computed from

$$\dot{s} = q_{\text{local}} \nabla C \qquad (14.13)$$

where ∇C is the gradient in silica solubility due to variation in pressure and temperature, and q_{local} is the local fluid flux. Silica solubilities (Fig. 14.2) were computed after Manning (1994), with water densities calculated using a modified Redlich-Kwong type equation. Pederson, Johansen and Wanger (Chapter 13) suggest a dis-equilibrium mechanism for advective silica transport in sedimentary basins, however such mechanisms are unlikely to operate in metamorphic systems

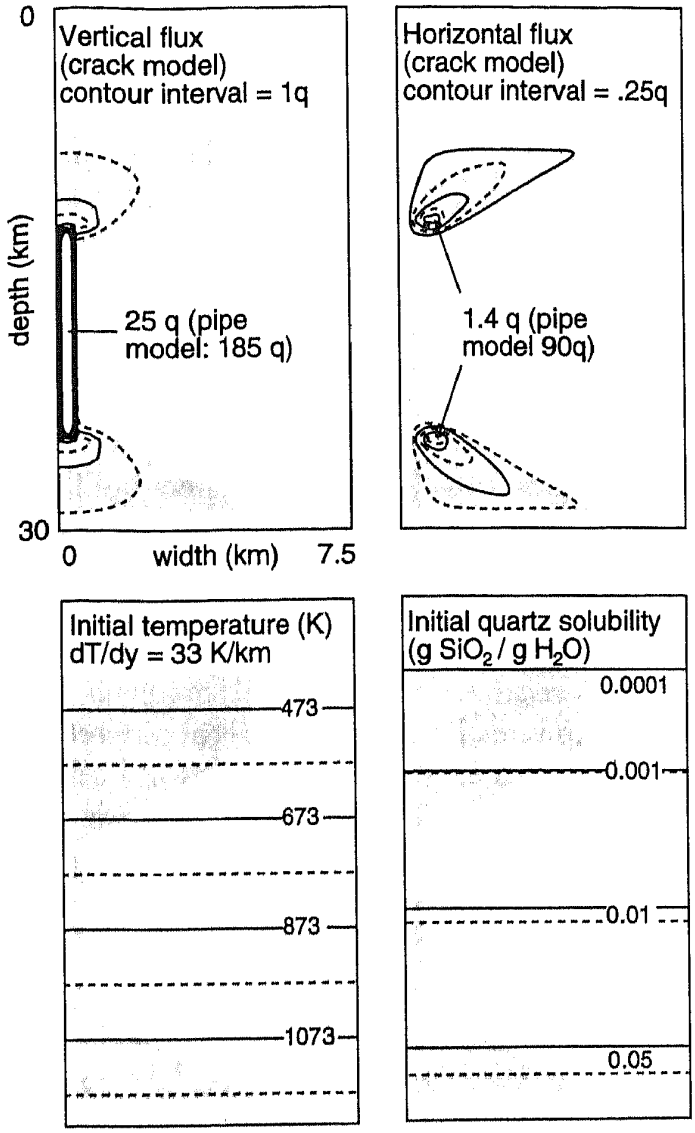

Figure 14.2 Initial model conditions. Vertical and horizontal flux components are shown for the crack model contoured in terms of the regional metamorphic flux q (equations 14.6 and 14.7), flux components vary more strongly in the pipe model. Silica solubilities (at quartz saturation, Manning, 1994) are shown at both lithostatic ($\rho_{rx}gy$) and hydrostatic ($\rho_f gy$) pressure.

because above *c.* 573 K excess silica precipitates almost instantaneously (e.g. Hemley *et al.*, 1980).

For a fracture zone to be an effective means of focusing fluid, fluid pressures must be below lithostatic, and would probably be very nearly hydrostatic. For this reason hydrostatic fluid pressures were used in all computations: as seen in Fig. 14.2, the effect of varying fluid pressures between the lithostatic and hydrostatic limits is relatively minor provided the pressure gradient is uniform; this effect becomes even less important for cooler geotherms. In reality it is likely that within the collection region fluid pressure outside of the fracture zone is closer to lithostatic. In this case the fluid will undergo pressure throttling during focusing. Such a throttling effect could cause a massive increase in the amount of quartz precipitated at the base of the fracture zone but would not appreciably change amount of silica transported within the upper portions of the fracture zone. Pressure throttling is unlikely to be a significant factor during dispersion for two reasons

1. dispersion will occur when the fracture zone passes through relatively permeable rocks and in such a regime it would be difficult to maintain large pressure gradients;
2. at lower temperatures the change in solubility even due to a lithostatic–hydrostatic fluid pressure drop is unimportant (Fig. 14.2, also Connolly and Thompson, 1989).

14.2.5 REGIONAL FOCUSING MODEL RESULTS: THERMAL EFFECTS

For a given geometry and focusing region width, the major sources of variation in the models are time and flow rate. Figure 14.3 shows the effect of time for models in which the regional flux is two orders of magnitude greater than the expected maximum q^*. For both geometries, the general form of the thermal anomaly associated with the fracture zone develops by *c.* 25 ka. With additional time, the volume of thermally perturbed rocks increases and temperatures increase slightly; but, by 200 ka the rate of temperature change slows substantially. In both models, the temperature perturbations are small in comparison to those reported by Chamberlain and Rumble (1988), and notably more so for the planar fracture model. Indeed, the temperature anomaly generated for the pipe model is more than four times that obtained for a similar focusing factors and background fluxes in the models presented by Brady (1989) and Hoisch (1991). This would seem to contradict the intuitive expectation that

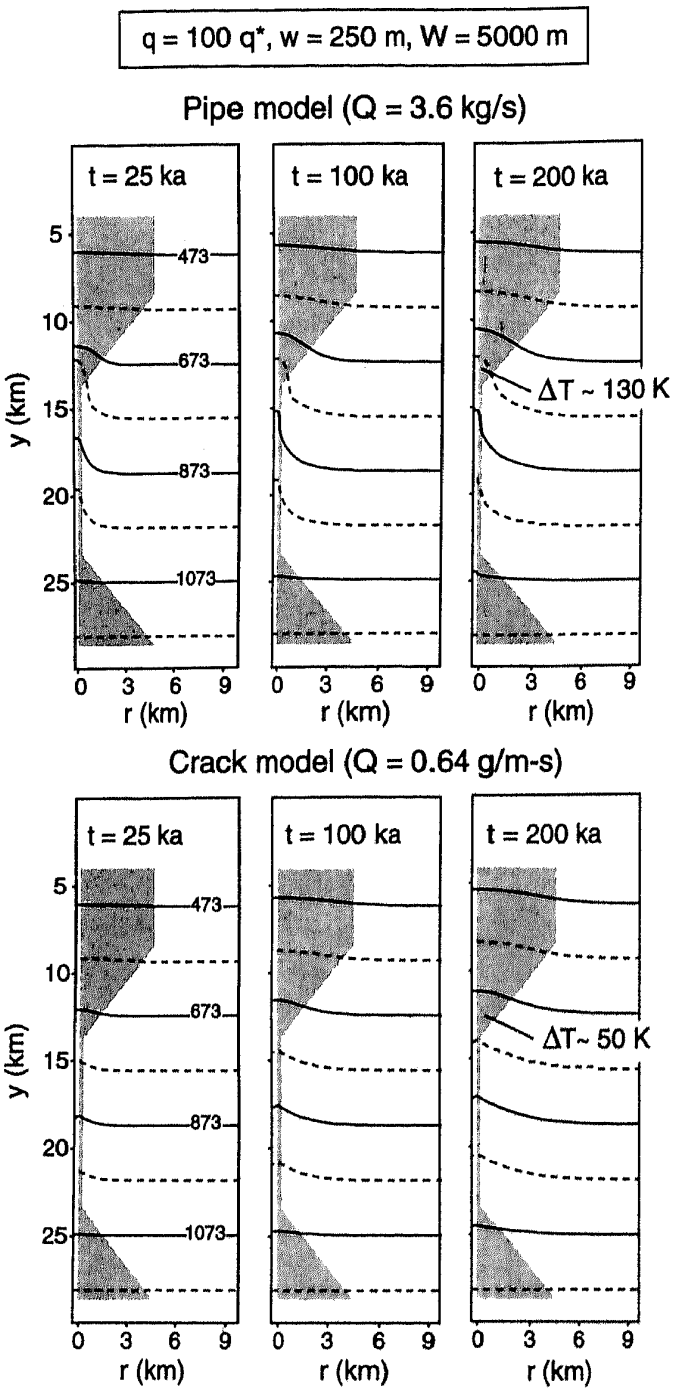

Figure 14.3 Temperature evolution as a function of time for a high regional fluid flux (100 q^*).

conductive heat loss from a radially symmetric fracture system should be greater than for a planar geometry (Brady, 1989); however, for a given focusing region width, radial focusing results in higher total fluxes, which is evidently a more important factor for the length scales considered here. The relatively rapid dispersion of heat and fluid flux for the radially symmetric model also causes the associated thermal anomaly to diminish more rapidly away from the vertical portion of the fracture zone.

Development of the thermal anomaly following the onset of fluid channelling can be seen more clearly in the temperature profiles along the pipe fracture zone axis (Fig. 14.4). Early in the model evolution an isothermal region develops almost instantaneously at the base of the fracture zone. Above this region the thermal gradient within the fracture zone is constant and identical to the unperturbed geothermal gradient. This behaviour reflects the fact that the down-temperature fluid flow must create a finite positive thermal anomaly. However, the consequent reduction in the thermal gradient increases the efficiency of heat convection by the fluid, so that the magnitude of thermal anomaly relative to the normal gradient will increase upwards. Provided vertical heat convection dominates over conduction, as is true for the flow rates chosen here, the flow will approach the isothermal limit. This isothermal region terminates when lateral heat conduction becomes comparable to the heat convection up the fracture zone for the initial geothermal gradient, i.e.:

$$QC_f \frac{dT}{dy} \approx 2(1 - p + p\pi w)k \frac{dT}{dr}, \quad (14.14)$$

thereafter flow occurs with the initial geothermal gradient, mimicking the models of Brady (1989) and Hoisch (1991). In the absence of perturbations to the conductive heat flow from the ends of the fracture zone, or from adjacent fractures, equation 14.14 can be used to estimate the position at which the transition from isothermal flow to flow with the initial thermal gradient occurs in the steady-state limit. For example, taking the planar fracture model with $Q = 0.63 \times 10^{-3}$ kg m^{-1} s^{-1} the total heat convection is 83 J m^{-1} s^{-1} for a vertical thermal gradient of 33 K km^{-1}, the lateral gradient necessary to accommodate this is then (83 J m^{-1} s^{-1})/2/k = 18 K km^{-1}. Assuming the lateral gradient away from the fracture zone is linear, then the isothermal flow would occur over a distance of *c.* 500 m above the fracture zone, in excellent agreement with the model illustrated

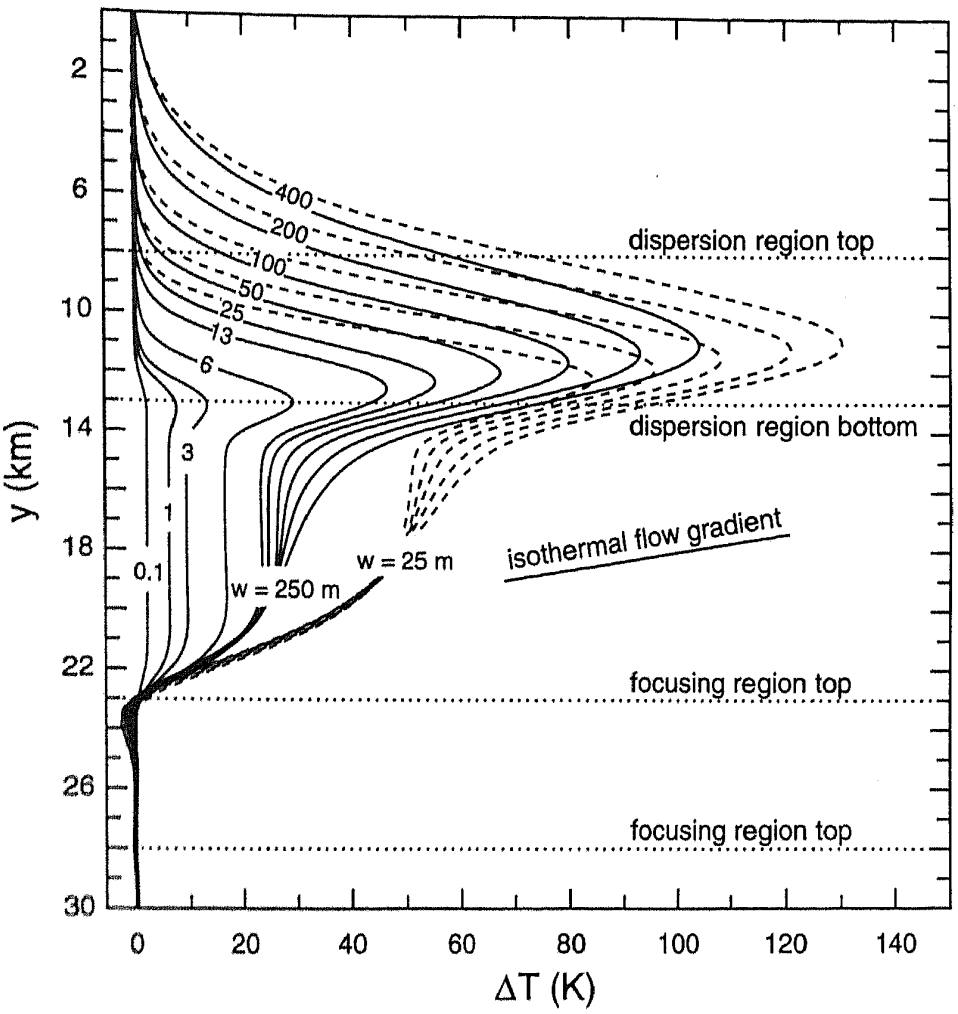

Figure 14.4 Differences between the temperature along the fracture zone axis and the unperturbed geotherm temperature for the pipe model as a function of time and fracture zone width. Model parameters are slightly different from those shown in Fig. 14.3: $Q = 1.2\,\mathrm{kg\,s^{-1}}$, $q = 10\,q^*$, and focusing and dispersion region half-widths of 9 and 3 km, respectively. Curves are labelled by time in ka; solid and dashed curves correspond to thermal anomalies for fracture zone widths of 500 and 50 m, respectively. Isothermal flow is very nearly realized at the transition from confined to dispersed flow and in the lower portion of the fracture zone.

in Fig. 14.3. The model results show that this quasi-steady state develops long before the effect of dispersion becomes important ($t \leqslant 25$ ka, Fig. 14.4).

Dispersion of the fluid results in a second region of nearly isothermal flow, which develops because the rate of heat convection into the dispersion zone overwhelms the capacity of the rock to conduct heat away, i.e. thermal throttling. This results in an isothermal shock front that propagates upward into the dispersion region. As this front advances, its area increases, but the total rate of heat convection remains constant, reducing the velocity of the front. Consequently fluid dispersion results in a heating effect similar to that from a two-dimensional heat source that expands and migrates upwards into the dispersion region. With time, the thermal anomaly within the dispersion region alters the nature of the heat flow within the fracture zone and perturbs the thermal gradient and quasi-steady state conditions attained earlier in the lower portions of the fracture zone. This in turn increases the ability of the fluid to transport heat and mass into the dispersion region, but this effect is countered by the increase in the volume of material that must be heated as the region of isothermal conditions broadens. In Fig. 14.4 it can be seen that the

increase in the temperature anomaly is about 10 K with a doubling of time, thus to achieve an anomaly of 150 K would require an additional time of at least 1.2 Ma. As discussed below it is unlikely fracture flow could be maintained on such time-scales because of silica precipitation.

The effect of an order of magnitude reduction in the fracture zone width increases the temperature anomaly for the pipe model by < 20 K (Fig. 14.4). This suggests that for fluid flow confined to fracture zones of $2w < 500$ m, the critical parameter is the total flow rate rather than flux. This can be justified given that the time-scale for heat conduction for such widths $\left(\tau = \frac{2w^2}{\kappa}\right)$ is on the order of hundreds of years, much less than that necessary for the development of a significant thermal anomaly by confined fluid flow. Despite the extraordinarily high regional flux used for the calculations, the maximum thermal anomaly is only 110 K in the dispersion region (Fig. 14.3), well below that necessary to explain the observations of Chamberlain and Rumble (1989). Figure 14.5 shows that the effect of reducing this flux to more plausible values is to make the thermal perturbation imperceptible as $q \rightarrow 10\,q^*$. Thus, from Fig. 14.5 it can be concluded that flow rates must exceed 0.1 kg s^{-1} to produce a significant thermal effect for the pipe model (for the crack model the critical flow rate is *c.* 0.1 g s^{-1} m^{-1}). For the model geometries shown, these flow rates correspond to thermal Peclet numbers for one-dimensional flow of the order of one, reflecting the relative importance of vertical heat flow.

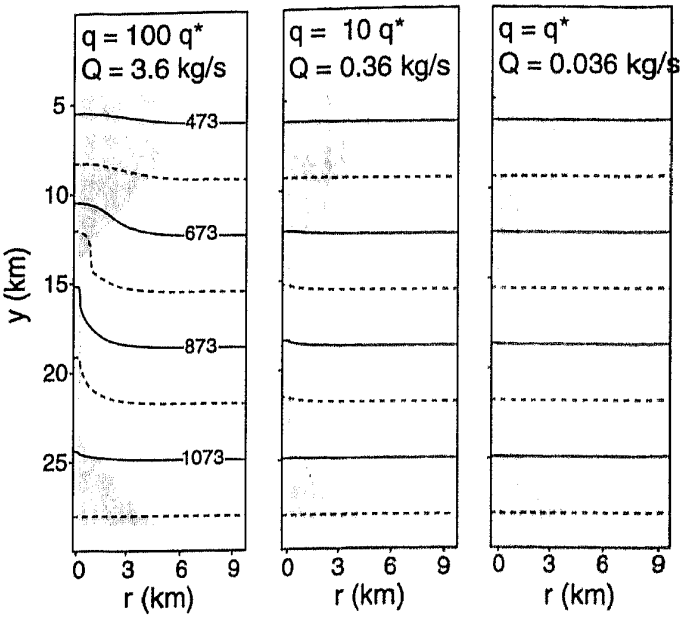

Figure 14.5 Effect of variation in regional flux for the pipe model at 200 ka. To a good approximation, variation in regional flux also can be used to simulate a change in the collection area (W_f). From equations 14.9 and 14.11 flow rates for a focusing radius of 5 km and regional fluxes of $10\,q^*$ and $0.1\,q^*$, are equivalent to flow rates for focusing radii of 15 and 2.3 km with a regional flux of q^*.

14.2.6 REGIONAL FOCUSING MODEL RESULTS: SILICA TRANSPORT

Earlier modelling (e.g. Yardley, 1986; Connolly and Thompson, 1989) has shown that the amount of quartz precipitated by pervasive, one-pass, fluid flow is inadequate to explain the quartz-veining in metamorphic rocks. As an alternative, Yardley (1986) suggested that silica transport by vertical, near-isothermal, fracture-controlled movement of relatively hot fluids into cooler overlying rocks could be responsible for quartz vein formation. However, the temperature profiles in Figs 14.3 and 14.4 demonstrate that extreme conditions are necessary to perturb the geothermal gradient within the fracture zone. Even when such conditions are realized, the models suggest that the geothermal gradient is unlikely to be reduced by more than 15 K km^{-1} except in the uppermost portion of the fracture zone (Fig. 14.4). Any reduction in the geothermal gradient must increase the amount of silica transported by the fluid into the region where the fluid is finally dispersed and cooled. Thus the amount of silica precipitated in the dispersion regions for the models (Fig. 14.6) is increased relative to that which would be precipitated by unfocused pervasive fluid movement. Because the change in quartz solubility with temperature is sensitive to the absolute temperature (Fig. 14.2), this increase is minor in comparison to the amounts of quartz precipitated within the fracture zone and focusing region.

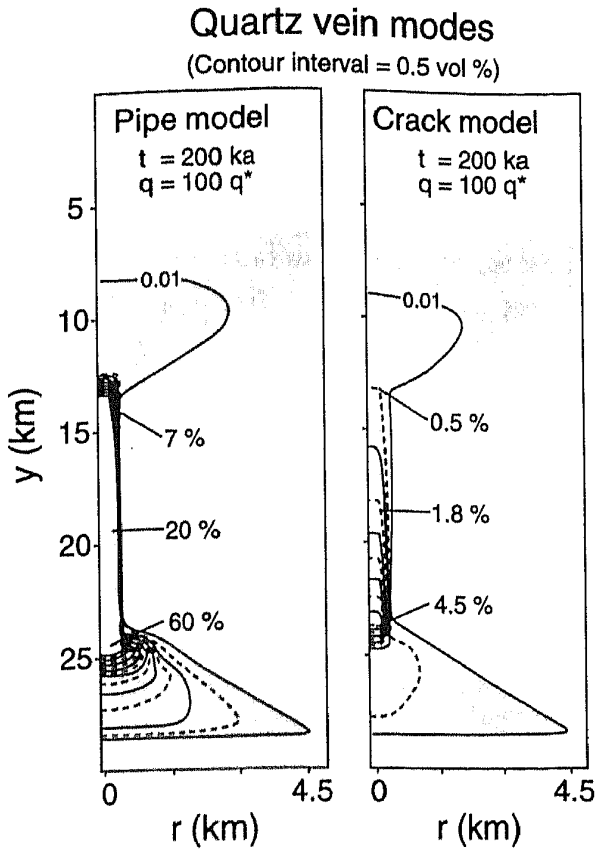

Figure 14.6 Amount of quartz precipitated for pipe and crack models after 200 ka. For clarity, contours of quartz modes greater than 7 volume % are not shown for the pipe model, these modes reach a maximum of *c.* 60% near the base of the fracture zone and drop smoothly to 7 volume % at the base of the dispersion region. Horizontal scale is twice the vertical scale.

Furthermore, the rapid cooling associated with dispersion is such an effective means of precipitating quartz, that the amount quartz veining that can be produced by such processes decreases drastically away from the fracture zone. The amounts of silica precipitated within the fracture zone are orders of magnitude greater than that necessary to fill any single fracture capable of accommodating the focused fluid flow. This suggests that, if such systems do exist, then they must be zones of active deformation and fracturing.

14.3 FORCED ADVECTION ABOVE A COOLING PLUTON

Granitic plutons are usually viewed as the heat engines responsible for driving free-convection, but they may also act as a source of intense, though ephemeral, fluid fluxes where free-convection is not possible. This section presents models constructed to examine the magnitude and scale of the effects that might arise from vertical channelling, and subsequent dispersion, of such fluids. At the outset, however, there are two reasons that it seems this is an improbable mechanism for generating the hotspots described by Chamberlain and Rumble (1988):

1. lower crustal plutons are unlikely to be generated by wet solidus melting (e.g. Wyllie, 1977), and therefore if they release large amounts of water, then the fluid will be released within 50–100 of the granite solidus (i.e. at temperatures too low, 923–1023 K, to form the hotspots);
2. to isolate advective heat effects, a plutonic fluid source would have to crystallize at depths of 5–10 km below the hotspot, which implies a cooler geotherm (15–20 K km^{-1}) than suggested by Chamberlain and Rumble's (1988) observations.

14.3.1 MODEL FOR CRYSTALLIZATION OF A GRANITIC PLUTON

A granitic (tonalite) pluton is assumed to be emplaced instantaneously at a depth of 20 km in rocks with an initial geotherm of 16 K km^{-1}. At emplacement the magma consists of 45 wt% melt phase with a water content of 6.7 wt%, at a temperature of 1013 K (T_0). The melt becomes water-saturated at 973 K (T_1), and releases water linearly with falling temperature to 923 K (T_2), at which point the melt is completely crystallized. Latent heat of crystallization (L, Table 14.1) is accounted for by expressing the specific heat of the magma as (Price and Slack, 1954):

$$C'_m = C_{rx} + \frac{X_m L}{T_0 - T_2} \qquad (14.15)$$

where X_m is the initial melt fraction. The enthalpic effect of fluid exsolution is taken to be zero (Clemens and Navrotsky, 1987). Heat loss due to removal of the fluid phase is approximated by

a further adjustment to the melt specific heat:

$$C''_m = C'_m + X_w X_m (C_f \rho_f - C'_m) \frac{T_1 + T_2}{2(T_2 - T_1)} \qquad T < T_1 \quad (14.16)$$

where X_w is the initial water fraction of the melt.

The fluid is assumed to be released at the base of a fracture zone which migrates downward as the melt crystallizes. Both pipe and crack model geometries were solved using boundary conditions and methods as described for the fluid focusing models. Non-steady state fluid flux terms (∇q) and free-convection of the magma were not considered. The crack models were done in 3-dimensional space to permit a finite fracture zone length.

14.3.2 COOLING PLUTON MODEL RESULTS

Model results for a spherical pluton of 5 km radius and pipe fracture zone of 900 m radius are summarized in Fig. 14.7. These show that initial flow rates (20–10 kg s^{-1}) generated by crystallization of a granitic pluton vastly exceed the rates necessary to overwhelm conductive heat transfer and generate advective heat anomalies. Once the initial thermal shock of emplacement has passed, fluid production rates drop in a roughly geometric progression with time so that the largest temperature anomaly in the dispersion region (*c.* 200 K) occurs essentially instantaneously with emplacement. For the relatively large pluton dimension chosen here, free-convection within the pluton might result in lower fluid production rates. However, calculations done for a smaller pluton, of 3 km radius, yield comparable thermal effects and fluid production rates (an average of 13 kg s^{-1} over 25 ka). Indeed it can be expected that the likelihood of preserving advective heat effects in metamorphic rocks will be larger with smaller plutons, because the conductive heat anomaly will be small.

For a 0.5 × 5.5 km planar fracture zone, all

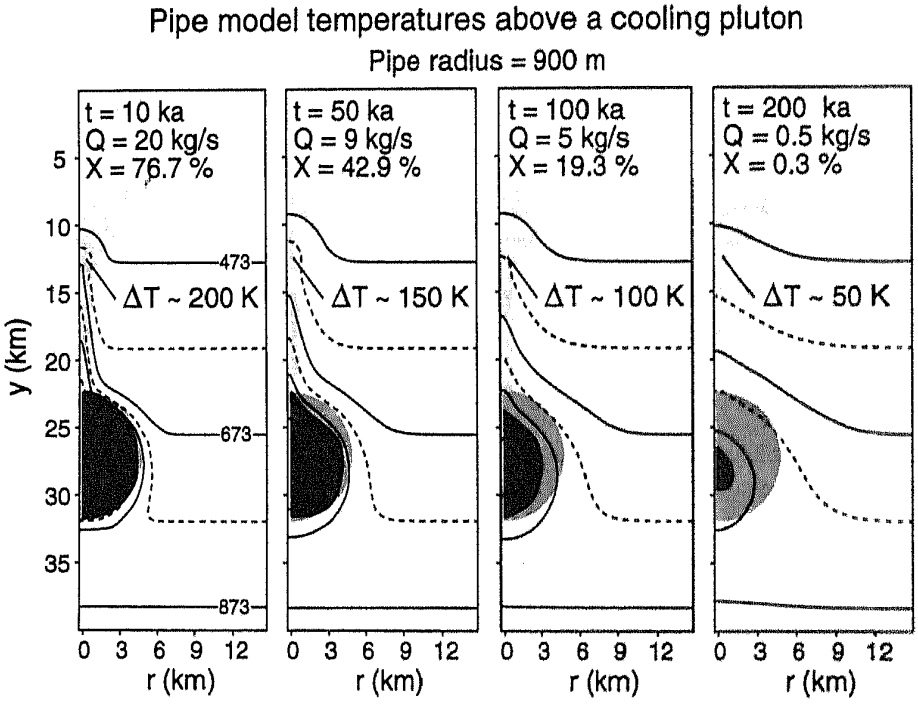

Figure 14.7 Temperature evolution following emplacement of tonalitic pluton assuming water released during crystallization is focused into a 1.8 km wide pipe-like fracture zone and dispersed 10 km above the pluton. Portions of the pluton at temperatures above fluid saturation, at fluid saturation, and fully crystallized indicated by light, heavy, and intermediate shading. *X* is the fraction of water remaining in the melt phase.

other model factors being identical to those for the calculation illustrated in Fig. 14.7, the magnitude of the advective heat effect is substantially smaller (Fig. 14.8). Consequently for this geometry, the maximum temperatures achieved occur late in the model history and are associated with conductive heat transfer.

The geothermal gradients in the pluton models are less extreme than those required for the extraordinarily high temperatures of the metamorphic reaction in the regional fluid focusing models presented earlier. Despite this, the most extensive silica precipitation occurs at depths where the confined flow originates rather than where it is dispersed. Because of the greater reduction in the geothermal gradient in the pipe model, the distribution of quartz is more uniform, but nonetheless unimpressive.

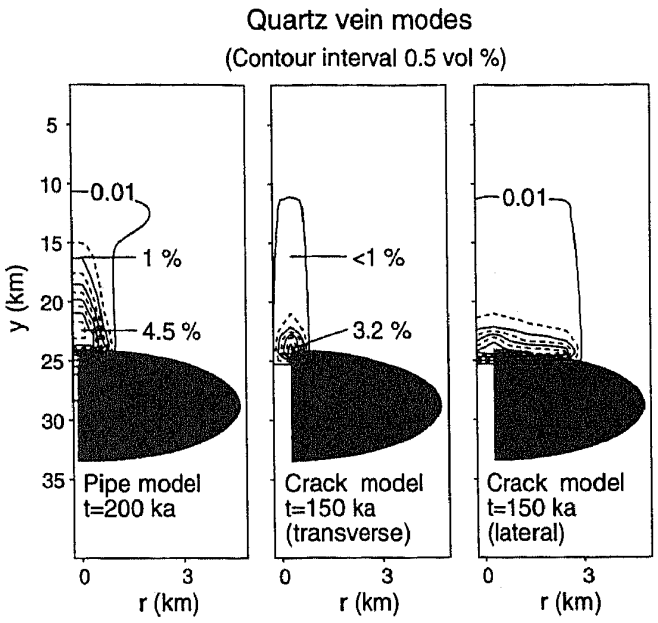

Figure 14.9 Distribution of quartz precipitated by forced convection through pipe and crack fracture zones above cooling plutons as in Figs 14.7 and 14.8. Horizontal scale is three times the vertical scale.

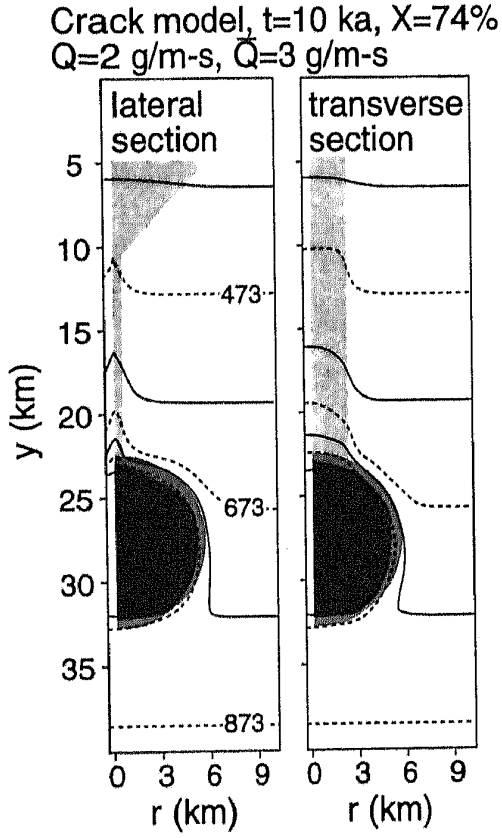

Figure 14.8 Temperature distribution 10 ka after emplacement of tonalitic pluton assuming water released during crystallization is focused into a 0.5 × 5.5 km planar fracture. Other parameters and labelling as in Fig. 14.7.

14.4 SUMMARY AND DISCUSSION

The models for focusing of regionally generated metamorphic fluids presented here differ from those of Brady (1989) and Hoisch (1991) in that collection and dispersion of the fluid and radially symmetric flow have been considered in detail. Radially symmetric flow is arguably a more appropriate model for the formation of phenomena such as the metamorphic hotspots described by Chamberlain and Rumble (1988). Likewise dispersal of fracture confined fluid flow would be necessary to form pervasive quartz veins within the hotspots, and more generally, to permit fluid–rock interaction. Both factors are shown here to substantially magnify the thermal effects of focused fluid flow, but the computed temperature anomalies are only significant if flow rate approaches 0.1 kg s^{-1} (pipe flow) or 0.1 g $m^{-1}s^{-1}$ (crack flow) on time-scales on the order of 10^4 a. Given that regional metamorphic fluxes are estimated to be on the order of 10^{-9} kg m^{-2} s^{-1}, radial focusing on a scale of 5–15 km would be necessary to generate such flow rates.

A fundamental limitation of such modelling is that it presumes the metamorphic process is continuous, but the lifetime of a large fracture zone is likely to be short in comparison to crustal metamorphic time-scales. Consequently, hydrothermal effects such as those observed by Chamberlain and Rumble (1988) may reflect periods of anomalously high fluid production, such as those which result from unstable systems (e.g. Yardley and Lloyd, 1995). The suggestion that lower crustal metamorphic reactions generate fluid pulses (Connolly and Ko, 1995), in which fluxes may be 50 times larger than steady-state fluxes, is a possible mechanism for reducing the radial focusing distance to as little as 2 km. Even so, lateral focusing on this scale seems improbable as it would require maintenance of large lateral pressure gradients and connected porosity at conditions where rocks are likely to deform rapidly, but this remains to be demonstrated. In contrast, the flow rates required to create detectable thermal effects are easily within the range that can be generated by the crystallization of mid-level granitic plutons. Conductive cooling of a granitic pluton with a radius of 3–5 km can produce fluid at rates of 10–20 kg s^{-1} for periods of 10–50 ka. Vertical channelling of this fluid, even in a relatively broad fracture zone of *c.* 1 km radius, over a distance of 10 km, may produce temperature anomalies of > 200 K. These effects and the predicted quartz-vein modes are similar to those observed in stock-works (e.g. Mickucki and Heinrich, 1993); however, granitic plutons are unlikely to produce water-rich fluid at temperatures above 873 K and thus cannot explain temperatures of this magnitude in Chamberlain and Rumble's (1988) metamorphic hotspots. The present modelling demonstrates that large-scale channelized vertical flow is capable of creating significant temperature anomalies, but the origin of Chamberlain and Rumble's (1988) hotspots, the best defined examples of anomalies generated by heat convection, remains enigmatic.

The ability of a hydrothermal fluid to transport a saturated solute such as silica is dependent both on the thermal gradient and, roughly, the log of the absolute temperature; however, the ability of the fluid to transport heat is virtually independent of the absolute temperature. Consequently, even if fluid fluxes can be attained that are adequate to produce advective anomalies, there is no reason to expect that the mass and heat anomalies will coincide in either time or space. This is demonstrated by the modelling here which shows that while extensive silification occurs in the lower portion of the fracture zone, little occurs when the fluid is dispersed after passing through the region where the thermal effects are most pronounced. This implies that such fracture systems would be choked at depth by silicification in relatively short time spans (< 25 ka) unless the fracturing is a continuous process. This effect would be accentuated by pressure throttling, which is most likely to be important when fluid enters the fracture zone. Thus it appears necessary to invoke free-convection or pressure solution to explain pervasive quartz veins in regionally metamorphosed rocks. This is in accord with many recent studies that have ascribed vein formation to local phenomena, rather than advective transport (e.g. Oliver *et al.*, 1993); Yardley and Botrell, 1992; Fisher and Brantley, 1992). In contrast, in sedimentary basins (Pederson, Johansen and Wangen, Chapter 13) and subduction zones (Manning, Chapter 8) fluid fluxes, and kinetic effects, may be large enough to allow significant silica transport.

ACKNOWLEDGEMENTS

I am grateful to M. N. Ozisik for introducing me to the numeric techniques used in this study; M. Casey for suggesting the dispersion model; and M. J. Bickle, B. W. D. Yardley, J. Ridley, and A. B. Thompson for helpful reviews and/or discussion.

APPENDIX: NUMERIC SOLUTION OF THE HEAT FLOW EQUATION

The heat flow equation, equation 14.12, was solved numerically using the Crank-Nicolson weighted finite difference method, second-order accurate centred differencing was used for the Laplacians, and upwind second-order accurate

differencing for gradients. In most calculations, numeric grid generation (Thompson, 1984) was used to enhance the accuracy of the solutions by permitting spatial resolution on a centimetre-scale in the vicinity of the fracture zones. By this technique the computational spatial domain described by a regular spaced grid in the variables $\zeta(r,y)$ and $\eta(r,y)$ which are non-linear functions of the true spatial coordinates r and y. This method reduces the error associated with conventional techniques for irregular grid spacing. The transformation between the computational and real spatial domains is defined such that:

$$\frac{\partial T}{\partial r} = \frac{1}{J}\left(\frac{\partial y}{\partial \eta}\frac{\partial T}{\partial \zeta} - \frac{\partial y}{\partial \zeta}\frac{\partial T}{\partial \eta}\right) \quad \text{(A.14.1)}$$

$$\frac{\partial T}{\partial y} = \frac{1}{J}\left(-\frac{\partial x}{\partial \eta}\frac{\partial T}{\partial \zeta} + \frac{\partial x}{\partial \zeta}\frac{\partial T}{\partial \eta}\right) \quad \text{(A.14.2)}$$

and

$$\nabla^2 T = \frac{1}{J^2}\left[\alpha\frac{\partial^2 T}{\partial \zeta^2} - 2\beta\frac{\partial}{\partial \eta}\left(\frac{\partial T}{\partial \zeta}\right) + \gamma\frac{\partial^2 T}{\partial \eta^2}\right] + \left[\nabla^2\zeta\frac{\partial T}{\partial \zeta} + \nabla^2\eta\frac{\partial T}{\partial \eta}\right] \quad \text{(A.14.3)}$$

where

$$\alpha = \left(\frac{\partial x}{\partial \eta}\right)^2 + \left(\frac{\partial y}{\partial \eta}\right)^2, \quad \beta = \frac{\partial x}{\partial \zeta}\frac{\partial x}{\partial \eta} + \frac{\partial y}{\partial \zeta}\frac{\partial y}{\partial \eta},$$

$$\gamma = \left(\frac{\partial x}{\partial \zeta}\right)^2 + \left(\frac{\partial y}{\partial \zeta}\right)^2,$$

$$J = \frac{\partial x}{\partial \zeta}\frac{\partial y}{\partial \eta} - \frac{\partial x}{\partial \eta}\frac{\partial y}{\partial \zeta}.$$

The metrics of the transformation are then determined from simultaneous solution of the finite difference approximation to the equations:

$$\nabla^2\zeta = P(\zeta,\eta) \quad \text{(A.14.4)}$$

$$\nabla^2\eta = Q(\zeta,\eta) \quad \text{(A.14.5)}$$

where $P(\zeta,\eta)$ and $Q(\zeta,\eta)$ are arbitrarily specified grid control functions used to attract the real grid points toward selected locations in the transformed coordinate space.

REFERENCES

Bickle, M. J. and McKenzie, D. (1987) The transport of heat and matter by fluids during metamorphism. *Contributions to Mineralogy and Petrology*, **95**, 384–92.

Bjørlykke, K., Mo, A. and Palm, E. (1988) Modelling of thermal convection in sedimentary basins and its relevance to diagenetic reactions. *Marine and Petroleum Geology*, **5**, 338–51.

Brady, J. (1989) The role of volatiles in the thermal history of metamorphic terranes. *Journal of Petrology*, **29**, 1187–213.

Chamberlain, C. P. and Rumble, D. (1988) Thermal anomalies in a regional metamorphic terrain: an isotopic study of the role of fluids. *Journal of Petrology*, **29**, 1215–32.

Clemens, J. C. and Navrotsky, A. (1987) Mixing properties of $NaAlSi_3O_8$–H_2O melt: new calorimetricdata and some geologic implications. *Journal of Geology*, **95**, 173–86.

Connolly, J. A. D. and Ko, S.-C. (1995) Development of excess fluid pressure during dehydration of the lower crust. *Terra Abstracts*, **7**, 312.

Connolly, J. A. D. and Thompson, A. B. (1989) Fluid and enthalpy production during regional metamorphism. *Contributions to Mineralogy and Petrology*, **102**, 346–66.

England, P. C. and Thompson, A. B. (1984) Pressure–temperature–time paths of regional metamorphism, I, Heat transfer during the evolution of regions of thickened crust. *Journal of Petrology*, **25**, 894–928.

Etheridge, M. A., Wall, V. A. and Vernon, R. H. (1983) The role of the fluid phase during regional metamorphism and deformation. *Journal of Metamorphic Petrology*, **83**, 205–26.

Ferry, J. M. (1987) Metamorphic hydrology at 13 km depth and 400–550°C. *American Mineralogist*, **72**, 39–58.

Fisher, D. M. and Brantley, S. L. (1992) Models of quartz overgrowth and vein formation: deformation and episodic fluid flow in an ancient subduction zone. *Journal of Geophysical Research*, **97**, 20043–61.

Fyfe, W. S., Price, N. J. M. and Thompson, A. B. (1978) *Fluids in the earth's crust*, Elsevier, Amsterdam.

Ganguly, J., Singh, R. N. and Ramana, D. V. (1995) Thermal perturbation during Charnockitization and granulite facies metamorphism in southern India. *Journal of Metamorphic Geology*, **13**, 419–30.

Hemley, J. J., Montoya, J. W., Marienko, J. W. and Luce, R. W. (1980) Equilibria in the system Al_2O_3–SiO_2–H_2O and some general implications for alteration mineralization processes. *Economic Geology*, **75**, 210–28.

Hoisch, T. D. (1991) The thermal effects of pervasive and channelized fluid flow in the deep crust. *Journal of Geology*, **99**, 69–80.

Jamtveit, B., Bucher-Nurminen, K. and Austrheim, H. (1990) Fluid controlled eclogitization of granulites in deep shear zones, Bergen Arcs, western Norway. *Contributions to Mineralogy and Petrology*, **104**, 184–93.

Manning, C. E. (1994) The solubility of quartz in H_2O in the lower crust and upper mantle. *Geochimica et Cosmochimica Acta*, **58**, 4831–9.

Mickucki, E. J. and Heinrich, C. A. (1993) Vein- and mine-scale wall-rock alteration and gold mineralisation in the Mount Charlotte deposit, Kalgoorlie, Western Australia. *Australian Geological Survey Organization Extended Abstracts*, **54**, 135–40.

Norton, D. and Knapp, R. (1970) Transport phenomena in hydrothermal systems: nature of porosity. *American Journal of Science*, **277**, 913–36.

Norton, D. and Knight, J. (1977) Transport phenomena in hydrothermal systems: cooling plutons. *Journal of Geology*, **277**, 937–81.

Oliver, N. H. S., Cartwright, I., Wall, V. J. and Golding, S. D. (1993) The stable isotope signature of kilometre-scale fracture dominated metamorphic fluid pathways, Mary Kathleen, Australia. *Journal of Metamorphic Geology*, **11**, 705–20.

Ozisik, M. N. (1985) *Heat Transfer*, McGraw-Hill, NY.

Peacock, S. M. (1987) Thermal effects of metamorphic fluids in subduction zones. *Geology*, **15**, 1057–60.

Peacock, S. M. (1989) Numerical constraints on rates of metamorphism, fluid production, and fluid flux during regional metamorphism. *Geological Society of America Bulletin*, **101**, 476–85.

Price, R. H. and Slack, M. R. (1954) The effect of latent heat on numerical solutions of the heat flow equation. *British Journal of Applied Physics*, **5**, 285–7.

Skelton, A. D. L., Graham, C. M. and Bickle, M. J. (1995) Lithological and structural controls on regional 3-D fluid flow patterns during greenschist facies metamorphism of the Dalradian of the SW Scottish Highlands. *Journal of Petrology*, **36**, 563–86.

Thompson, J. F. (1984) Grid generation techniques in computational fluid dynamics. *American Institute of Aeronautics and Astronautics Journal*, **22**, 1505–23.

Thompson, P. H. (1989) Moderate overthickening of thinned sialic crust and the origin of granitic magmatism and regional metamorphism in low-P–high-T terranes. *Geology*, **17**, 520–3.

Walther, J. V. and Orville, P. M. (1982) Volatile production and transport in regional metamorphism. *Contributions to Mineralogy and Petrology*, **79**, 252–7.

Wyllie, P. J. (1977) Crustal anatexis: an experimental review. *Tectonophysics*, **43**, 41–71.

Yardley, B. W. D. (1986) Fluid migration and veining in the Connemara Schists, Ireland, in *Fluid–Rock Interactions during Metamorphism*, (eds J. V. Walther and B. J. Wood), Springer, New York, pp. 89–108.

Yardley, B. W. D. and Bottrell, S. H. (1992) Silica mobility and fluid movement during metamorphism of the Connemara schists, Ireland. *Journal of Metamorphic Geology*, **10**, 453–64.

Yardley, B. W. D. and Lloyd, G. E. (1995) Why metasomatic fronts are really sides. *Geology*, **23**, 53–6.